REFURBISHMENT AND CHARACTERISATION OF THE OXFORD LOW DENSITY HYPERSONIC WIND TUNNEL

Donaldson, N., Doherty, L., Ivison, W., Wilson, C. F., McGilvray, M., Ireland, P. T.

Oxford Thermofluids Institute
University of Oxford
Southwell Building, Osney Mead, Oxford, UK, OX2 0ES

ABSTRACT

In the study of atmospheric entry, one of the most challenging environments to model is the lower phase of the transition regime between free molecular and continuum behaviour. This regime, known as slip flow, occurs at Knudsen numbers between 0.001 and 0.1, i.e. when the mean free path of the gas around an object starts to become significant compared to said object's physical dimensions. The Oxford Low Density Wind Tunnel is a continuous flow facility specifically designed to model this regime (at Mach numbers in the range $5 \leqslant Ma \leqslant 10$) which has recently been re-commissioned with a range of new subsystems including upgraded instrumentation. This paper presents experimental flow characterisation measurements for two conditions, specifically Mach 5 flows at $Kn = \{0.006\dot{6}, 0.02\}$, performed using Pitot pressure and total temperature surveys. These results confirm the suitability of the wind tunnel for simulating hypersonic slip flow problems such as those associated with atmospheric entry calculations.

Index Terms— Hypersonic, experiments, ground test facility, characterisation

1. INTRODUCTION

The Oxford Low Density Tunnel (LDT)[1]is an open-circuit, continuous flow wind tunnel designed to simulate rarefied hypersonic conditions relevant to entry into planetary atmospheres. The facility comprises a three stage vacuum pumping system capable of operating using any inert compressed gas, and is able to run continuously for timescales of the order of hours. Following a period of inactivity, the LDT has recently been refurbished, upgraded, and recommissioned. Additions and improvements to the facility include new traversing mechanisms (3 linear axes and 2 rotational axes), a new data acquisition system, high temperature seals, and a water cooling system designed to mitigate boundary layer growth in the contoured nozzle (hence increasing the size of the experimental plume's core flow region).

[1] `http://oti.eng.ox.ac.uk/facilities/low-density-tunnel/`

The purpose of this study is to characterise the flow generated by the LDT in support of current and future research activities utilising the facility. These activities have most recently consisted of low enthalpy thermal flux surveys on satellite debris analogues towards the improvement of atmospheric entry simulations. The environment of the lower transition regime (otherwise known as the slip regime, where $0.001 \leqslant Kn \leqslant 0.1$) is of particular interest in this regard, as it is in this regime that thermal "pre-soaking" [1] occurs prior to the onset of the continuum regime (where $Kn < 0.001$).

The range of Mach numbers achievable in the LDT is typically $5 \leqslant Ma \leqslant 10$, depending on nozzle choice. While these are significantly lower than the Mach numbers reached during atmospheric entry (of the order of 30 in some cases), they are considered representative since the dependence of thermal behaviour, aerodynamic coefficients, shock structures, etc. on Mach number decreases progressively in the hypersonic regime (where $Ma \leqslant 5$) [2].

2. FACILITY DESCRIPTION

The LDT is an extremely versatile experimental facility, and has previously been used for a variety of different studies. These include, but are by no means limited to: fundamental research into hypersonic flow over spheres and cones, the development of an anemometer for Mars landers, and most recently, research into heat flux distributions on cylinders during atmospheric re-entry (in support of the study of satellite debris demise).

The primary components and instrumentation of the LDT test chamber, stagnation chamber, and gas conditioning system are shown in Figure 1.

2.1. Control and measurement instrumentation

Control of the total temperature of the working gas is accomplished via an inline heater and heated jacket around the stagnation chamber. These are connected to a pair of PID controllers, which are informed of their respective component's temperatures by a corresponding pair of K-type thermocouples. The first of these controls the inline heater using

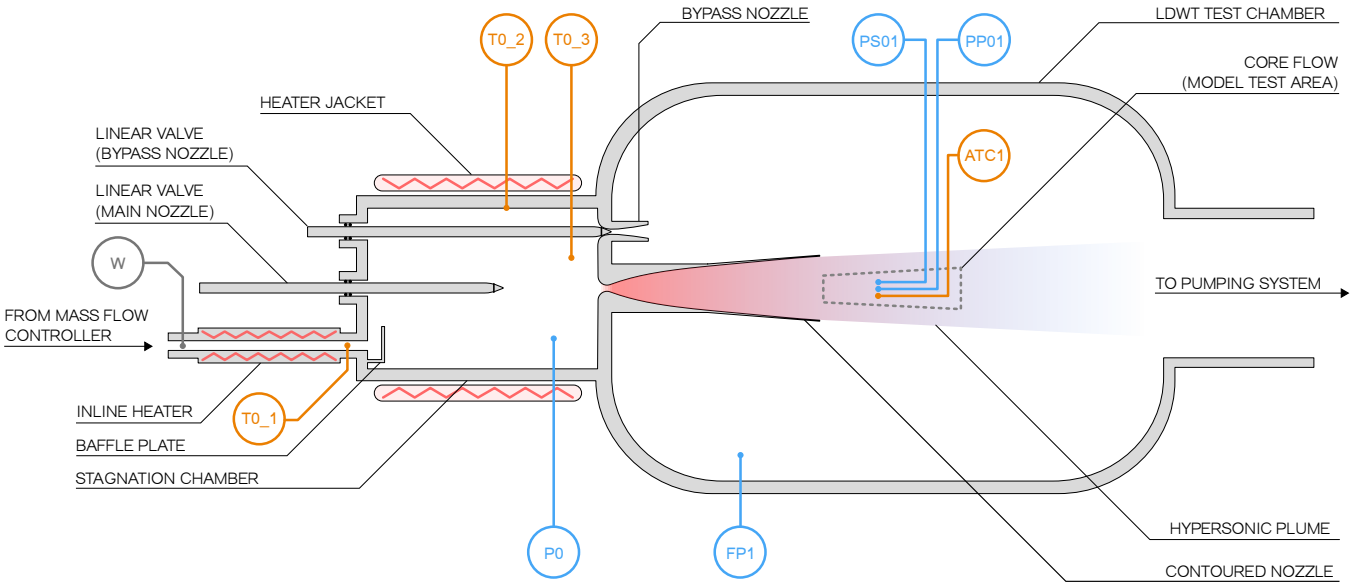

Fig. 1: Instrumentation installed in the LDT test chamber. Red sawtooth patterns denote electric heaters. Coloured bubbles denote the following types of instrumentation: blue, pressure; orange, temperature; grey, flowrate.

the temperature reading of thermocouple T0_1, which is suspended inside the outlet of the heater immediately upstream of the stagnation chamber. The second PID controls the heater jacket around the stagnation chamber by reading thermocouple T0_2, which is spot-welded to the interior of the stagnation chamber wall. A third thermocouple (T0_3), which measures the gas total temperature for post processing, is suspended inside the stagnation chamber on a stainless steel rod, approximately 1/4 of a radius away from the chamber centreline.

The final piece of temperature instrumentation shown in Figure 1 (ATC1) is a thin-wire aspirated thermocouple based on that developed by Widodo and Buttsworth [3]. It features a cylindrical annulus manufactured from rohacell with the aforementioned thermocouple draped across the opening. This device is used to stagnate the hypersonic flow from the contoured nozzle, allowing the total temperature to be measured in the subsonic post-shock region near the surface of the aspirated body.

The background pressure in the test chamber is measured using transducer FP1, while the stagnation chamber pressure is measured using P0. Plume surveys are performed using transducers PP01 and PS01 (Pitot and static measurements, respectively). Transducer FP1 is a wide range Pirani sensor, and is utilised by the LDWT control system, while PS01, an Inficon with a range of 133 Pa (1 $Torr$), is utilised for static pressure, p_∞, measurements. Pitot pressure, p_0, measurements in the stagnation chamber are taken by transducer P0, which is a Baratron (an absolute capacitance manometer) with a range of 13300 Pa (100 $Torr$). Sensor PP01 is also a Baratron, but features a measurement range of 1330 Pa (10 $Torr$), one order of magnitude smaller than P0. The inlet mass flow rate (measurement label W in Figure 1) is controlled using an Omega mass flow controller with a maximum flowrate of 50 $SLPM$ ($\sim 1.0\,g/s$).

The contoured nozzle chosen for the present study has previously been utilised by both Dahlen [4] and Owen [5]. This nozzle is used for the present work such that a Mach number beyond the hypersonic limit may be achieved whilst still maintaining a reasonable degree of uniformity within the plume.

The initialisation of the hypersonic plume involves setting the mass flow controller and supplying power to the heaters. The bypass nozzle valve (see Figure 1) is then opened while the main nozzle valve remains closed, allowing the pressure and temperature in the stagnation chamber to rise to a steady state. When an experimental run is to start, the tunnel operator closes the bypass valve whilst simultaneously opening the main nozzle valve, essentially switching the flow from the bypass nozzle to the main nozzle. This condition is shown in Figure 1.

While the above method of flow initialisation can be used to produce a step change in flow rate (and hence freestream conditions) for a test article in the LDT, it can lead to temperature fluctuations due to the temporary disruptions in flow rate as the valves are operated manually. To avoid this, two alternate methods of effectuating a step change in flow can be utilised. These allow fluctuations in test stagnation conditions caused by the manual operation of the linear valves to be reduced.

The first of these involves a “flow shield” (not pictured in Figure 1) which may be positioned a short distance in front of the nozzle, thereby blocking the flow from interacting with

anything immediately behind it. The shield may subsequently be removed from the plume by activating an attached stepper motor, thus allowing any test articles behind the shield to immediately be exposed to the nozzle plume. The second initialisation method operates in the opposite fashion; test articles are initially positioned outside of the hypersonic plume and are subsequently manoeuvred into the flow using a linear traversing mechanism. Unlike the first method, this procedure allows the plume to be fully established and in a steady state prior to the start of an experiment. However, it also requires the use of at least one of the LDT's dedicated traversing motors, while the flow shield used in the first method is a standalone piece of equipment.

2.2. Traversing mechanism

The LDT features a dedicated traversing mechanism comprising five stepper motors and two mounting platforms. Although the traverses are reconfigurable, there are three distinct modes which have previously been utilised during experiments. These are a 3-axis linear arrangement (X, Y, and Z axes), a 2-axis rotational arrangement (pitch and yaw axes), and a 4-axis hybrid arrangement (X, Y, Z, and pitch axes).

The former of these configurations, i.e. the 3-axis linear arrangement, was utilised for the present work, and is shown in Figure 2. The contoured nozzle is also included, as are the coordinate systems assigned to each. the traverse coordinate system denotes the directions used for the input of motion commands to the traverse controller, while the nozzle coordinate system is used for the presentation of results. As such, all subsequent flow characterisation plots utilise the nozzle coordinate system for their spatial axis.

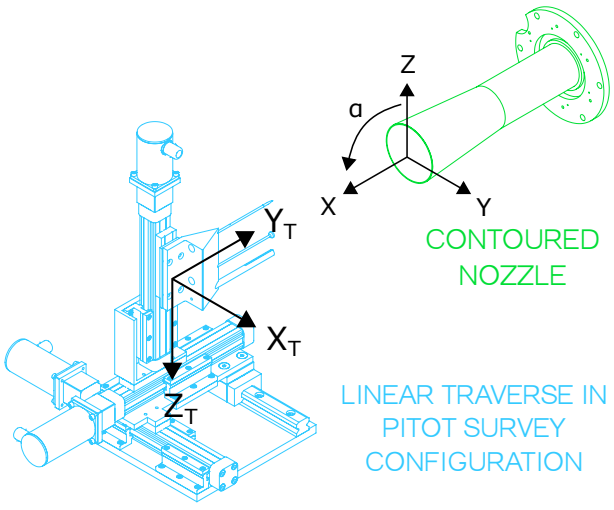

Fig. 2: Coordinate systems assigned to the nozzle and linear traversing mechanism.

2.3. Pitot rake

A new Pitot rake was designed and manufactured for the present work, a CAD drawing of which is shown in Figure 3. The wedge-shaped mounting block is affixed to the carriage of the linear traverse mechanism as shown in Figure 2, while measurement probes protrude from the apex of the wedge. These probes are, from top to bottom, a static pressure probe, a Pitot probe, and an aspirated thermocouple (PS01, PP01, and ATC1, respectively, in Figure 1). Attachment points for flexible hoses (utilising the ISO-KF vacuum fitting standard) are present on the rear face of the wedge, and are used to connect the Pitot rake to externally mounted pressure transducers.

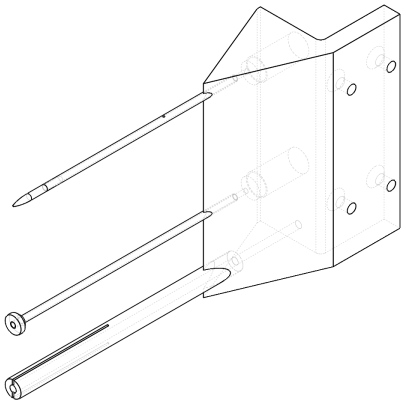

Fig. 3: Isometric CAD drawing of the Pitot rake.

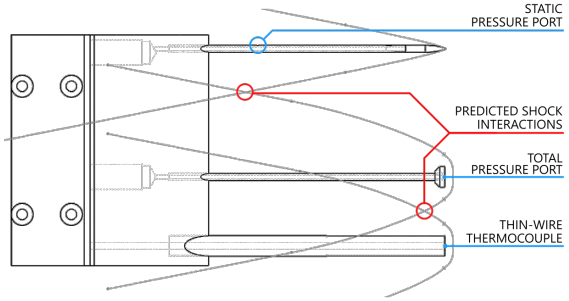

Fig. 4: Predicted shock interactions on the traverse Pitot rake at a freestream Mach number of 2

The lengths of the probes were defined according to the results of a series of axisymmetric RANS CFD simulations run using ANSYS FLUENT. These analyses were performed separately for each of the three probes, and the resulting shock structures overlaid in CAD such that flow interactions could be accounted for. Figure 4 shows these simulated structures for a low Mach number case ($Ma = 2$), the freestream conditions for which were derived from LDT measurements (with

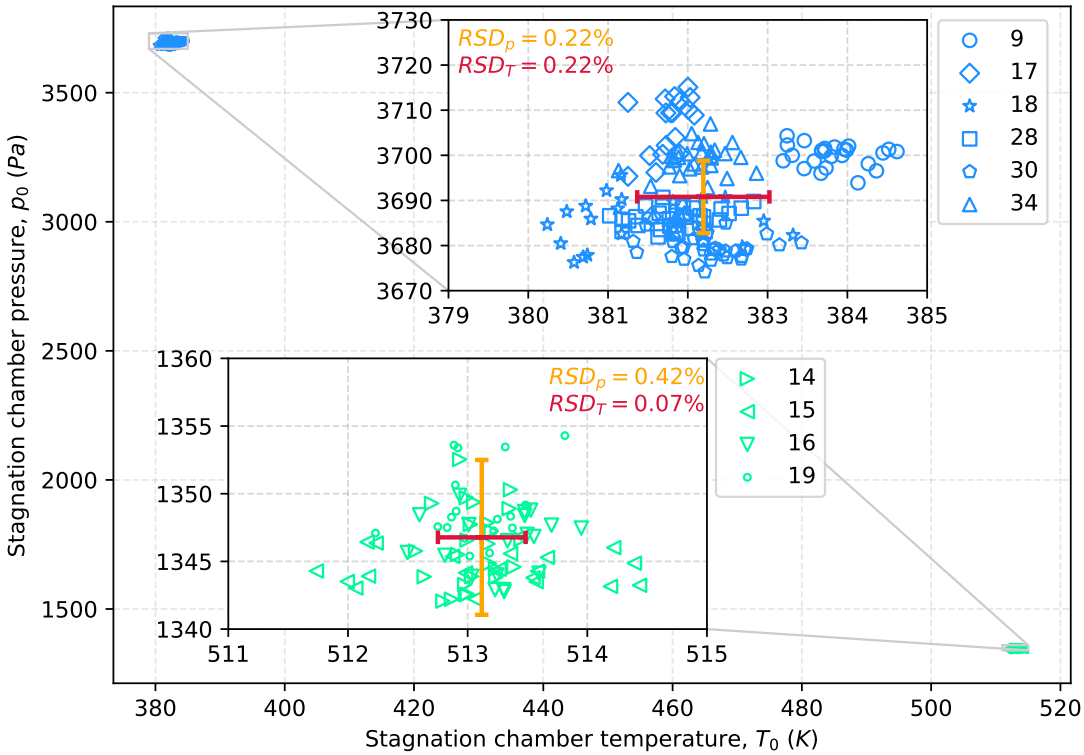

Fig. 5: Stagnation conditions in the LDT gas conditioning system averaged over several separate runs. Blue markers represent runs with a nominal Knudsen number of $0.006\dot{6}$, while green markers represent a nominal Knudsen number of 0.02. Legend indices denote individually numbered LDT runs, i.e. 4 runs are presented at the $Kn = 0.02$ condition, and 6 at the $Kn = 0.006\dot{6}$.

the exception of velocity, which was scaled artificially in order to alter Ma whilst maintaining a realistic Kn).

This low Mach number was selected such that the shock structures would be larger than those expected at nominal LDT flow conditions, thus representing a "worst case" for potential shock structure interactions. Even at this low Mach number — which would only occur in the LDT towards the outer extremities of the experimental plume — it may be observed that no interactions occur sufficiently close to the probes' measurement locations to interfere with their operation.

3. EXPERIMENTAL PROCEDURE

During a typical characterisation run in the LDT, the plume generated by the contoured nozzle is surveyed using the linear traversing mechanism and Pitot rake described in Sections 2.2 and 2.3, respectively. A table of points in the traverse coordinate system (see Figure 2) are entered into the LDT control system (a National Instruments PXI series DAQ running LabView) as a CSV file. For the present work, all points lay in a plane perpendicular to the nozzle's flow axis (direction x in Figure 2) situated $15\,mm$ downstream of the nozzle exit. The traversing mechanism is then centred relative to the nozzle exit using a pair of self-levelling line lasers positioned perpendicular to one another in the test chamber.

Once the flow through the nozzle has reached a steady state, the DAQ program is started, in turn directing the traverse to move to the points in the coordinate list in sequence. Once the traverse begins its move operation, the DAQ program waits until the stepper motors report that their motion has ceased. At this stage, the Pitot rake is stationary in the flow at the desired position, and data acquisition is triggered. The readings of each of the sensors shown in Figure 1 are recorded at a sampling rate of $200\ Hz$ for a predetermined time (selectable by the operator), and saved to the DAQ's internal hard drive.

The resulting data comprises a series of tables of various sensor readings against time; one for each point in the aforementioned CSV file of spatial coordinates. A series of post-processing scripts are then utilised to appropriately sort, filter, trim, and average these data. For the plots presented herein, the data acquired at each point in the coordinate table were trimmed to omit any readings acquired prior to the sensors equilibrating with the plume, i.e. prior to a given reading achieving a well-defined steady state. Signal noise was generally low throughout all runs, but was further mitigated during post-processing using a Savitzky-Golay filter of order 2 and window length $\frac{N}{100}$, where N was the total number of samples recorded.

4. EXPERIMENTAL CHARACTERISATION

For flow characterisation, the results of multiple LDT runs at two conditions are presented, both of which were selected based upon Knudsen number (calculated using Eq (1) and a representative length scale, L, of $10\,mm$). The two selected Knudsen numbers, along with their respective inlet conditions are presented in Table 1. Note that the mass flowrate, w, and the stagnation chamber temperature set-points are the two primary input conditions that an operator may select.

$$Kn = \frac{\mu\sqrt{\pi RT}}{pL\sqrt{2}} \tag{1}$$

Table 1: Flow and stagnation conditions for the two different cases examined during the characterisation activities (averaged over all runs). Knudsen numbers were calculated with $L = 10\,mm$

Cond.	Ma	Kn	$\overline{p_0}$	$\overline{T_0}$	$\overline{w}$
—	—	—	(Pa)	(K)	$(SLPM)$
1	5.46	~~0.0066~~	3690.79	382.19	28.438
2	5.00	~~0.02~~	1346.78	513.12	9.86

The readings of sensors PP01 and T_01 (see Figure 1) averaged over each separate LDT run are presented in Figure 5. As may be observed, the consistency of stagnation quantities in the LDT is generally excellent, indicating a high degree of experimental temporal stability (low scatter during a single run) and experimental repeatability (repeatability between separate runs). The relative standard deviation (RSD), i.e. the ratio of a data set's standard deviation to its mean, is also plotted for both stagnation quantities. As one would expect, the RSD is uniformly low for LDT stagnation conditions, with maximum values of 0.42% and 0.22% for p_0 and T_0, respectively.

Scatter plots of the flowfield Pitot pressure, p_T, and total temperature, T_0, sampled during the characterisation runs are presented in Figures 6a and 6b, respectively. A third plot showing the ratio between the Pitot pressure, p_T, and stagnation chamber pressure, p_0, for each run is presented in Figure 6c. The horizontal axis of each of these figures represents the radial distance from the nozzle centreline to the position of a given reading. These values were calculated using the positions of the Pitot probe in the nozzle coordinate system (see Figure 2). The X direction was omitted since all readings were recorded in a plane $15\,mm$ downstream of the nozzle exit, hence resulting in all X coordinates being identical across individual runs.

Referring to the low Kn run data presented in Figure 6a, it is clear that there is a "core flow" region of uniform Pitot pressure, p_T, which manifests from the nozzle centreline out to a radius of $\sim 15\,mm$. The Pitot pressure ratio, $\frac{p_T}{p_0}$, (presented in Figure 6) is similarly uniform, indicating that the freestream Mach number in this region is also uniform. This trend is replicated in 6b, where a region of uniform total temperature, T_0, extends from the nozzle centreline out to a radius of $\sim 20\,mm$.

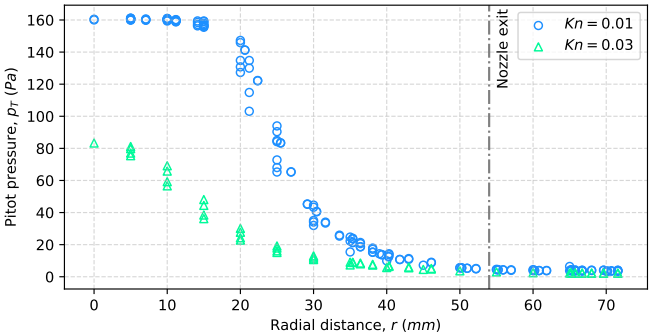

(a) Pitot pressure, p_T

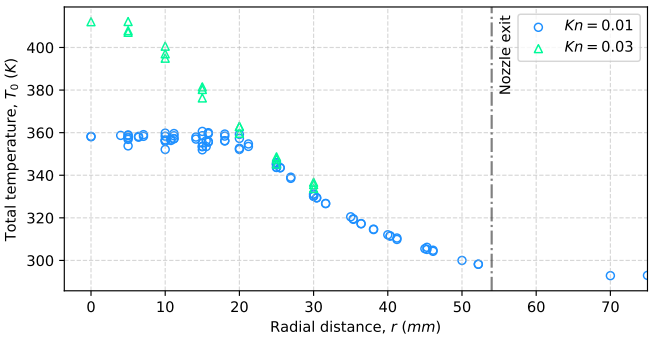

(b) Total temperature, T_0

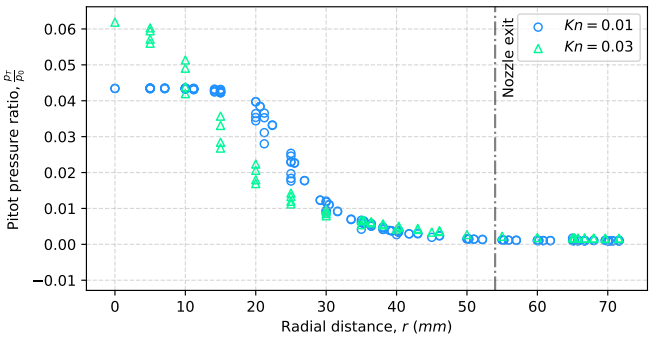

(c) Pressure ratio, $\frac{p_T}{p_0}$

Fig. 6: Plots of measured Pitot pressure, total temperature, and Pitot-stagnation pressure ratio in the LDT nozzle plume $15\,mm$ downstream of the nozzle exit. Data are plotted against the radial distance, r, from the nozzle centreline.

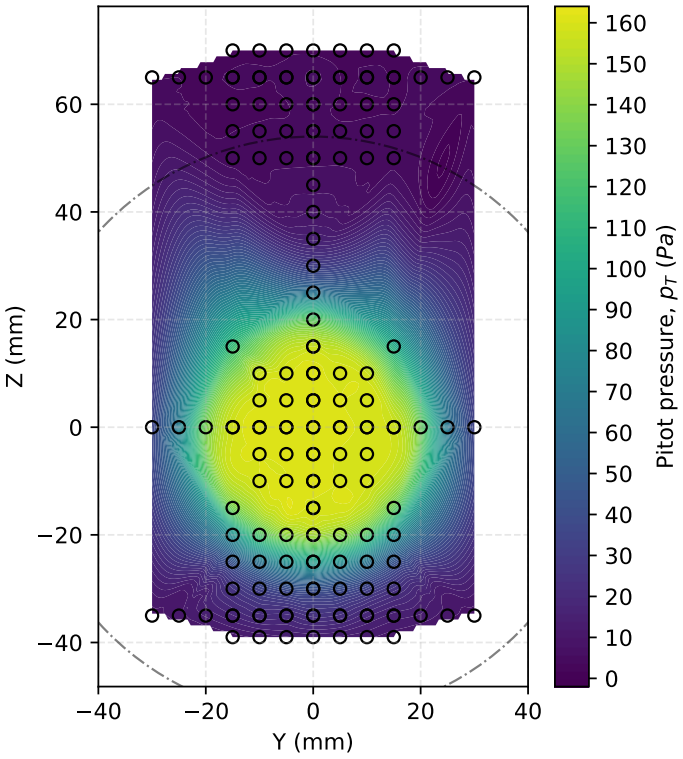

(a) $Kn = 0.006\dot{6}$

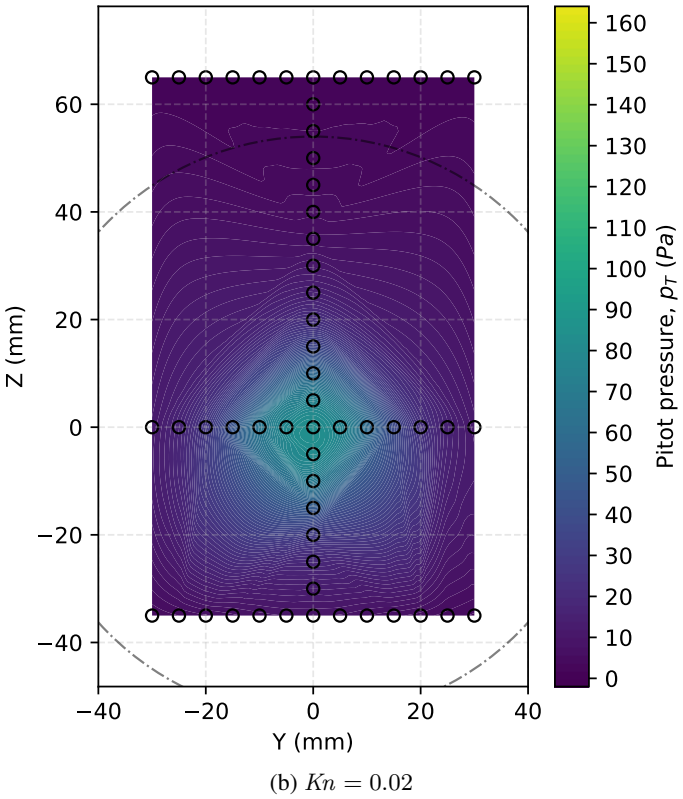

(b) $Kn = 0.02$

Fig. 7: Contours of Pitot pressure 15 mm downstream of the nozzle mouth in the LDT. Black circles indicate sampling locations, and the large black ring indicates the boundary of the nozzle wall. The contour surface is plotted using 2D cubic spline interpolation.

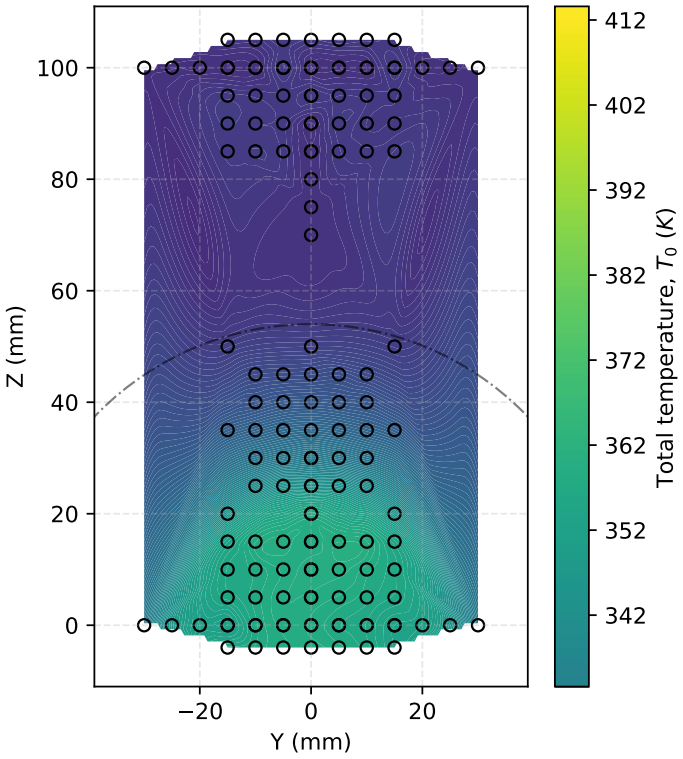

(a) $Kn = 0.006\dot{6}$

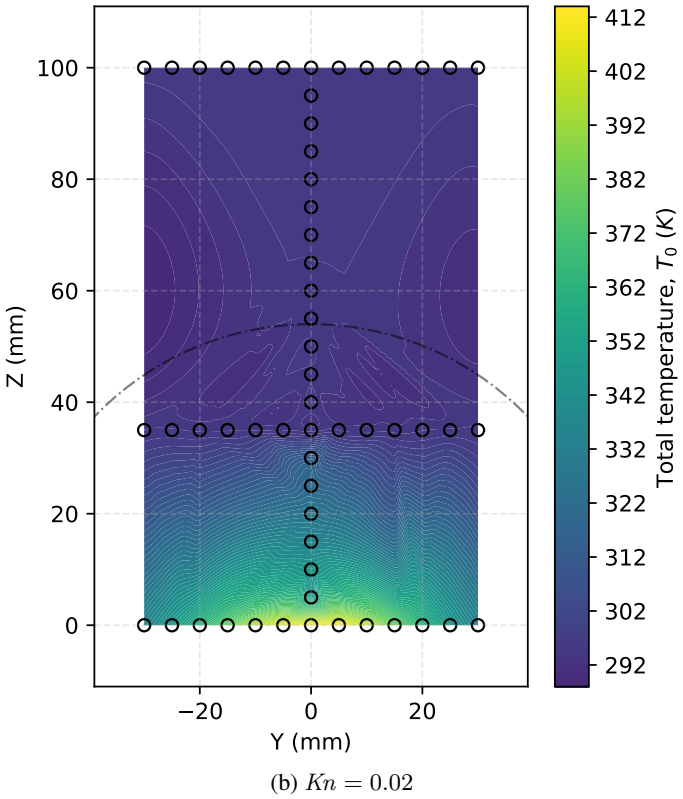

(b) $Kn = 0.02$

Fig. 8: Contours of total temperature 15 mm downstream of the nozzle mouth in the LDT. Black circles indicate sampling locations, and the large black ring indicates the boundary of the nozzle wall. The contour surface is generated using 2D piecewise cubic interpolation.

The high Kn runs' core flow region, however, is far smaller than that of the low Kn runs, as is evidenced by the Pitot pressure and total temperature data presented in Figures 6a and 6b, respectively. Both p_T and T_0 readings for the high Kn runs peak at the nozzle centreline, but as opposed to the low Kn runs, almost immediately begin to decrease with increasing radial distance, r. A small region of near-uniform flow may be observed in the range $0 \leqslant r < 5\,mm$, although it must be acknowledged that p_T readings in this area show significant scatter compared to the low Kn cases. As such, the level of flow uniformity evident in the low Kn runs cannot be said to be present at this condition. The ratio $\frac{p_T}{p_0}$ presented in Figure 6c also decreases in this fashion, indicating that the core Mach number for the high Kn runs also decreases steeply as $r \uparrow$.

Equation (2) shows the relationship between the total pressures downstream and upstream of a normal shock. Using a simple iterative approach, this equation may be solved to find the Mach number that results in a given pressure ratio. Assuming that the upstream total pressure, p_{0_1}, in the LDT plume is approximately equal to the stagnation chamber pressure readings, p_0, substituting in Pitot pressure measurements from the Pitot rake, and setting $\gamma = 1.4$, an estimate of the plume Mach number may be calculated. This procedure will produce the most accurate estimate at the nozzle centreline, i.e. where the total pressure is likely to be highest, and hence closest to the stagnation chamber pressure. Performing these calculations for the mean values of p_0 and p_T from both sets of runs results in approximate core flow Mach numbers of 5.47 and 5.00 (rounded from 4.997) for the low and high Kn runs, respectively.

This method of calculation was also used in order to determine the freestream Knudsen numbers for the two separate sets of LDT inlet conditions shown in Table 1. Using the Mach numbers derived from the pressure ratio calculation, the static pressure and temperature of the core flow were estimated, and hence the Knudsen number was calculated (using Eq. (1) and the NASA Sutherland-Keyes viscosity model). Appropriate inlet conditions for a target Knudsen number could then be selected at will, and used by the LDT operator to establish an operating point which would then be maintained throughout each individual run.

$$\frac{p_{0_2}}{p_{0_1}} = \left[\frac{(\gamma+1)\,Ma^2}{(\gamma-1)\,Ma^2+2}\right]^{\frac{\gamma}{\gamma-1}} \left[\frac{\gamma+1}{2\gamma\,Ma^2-\gamma+1}\right]^{\frac{1}{\gamma-1}} \quad (2)$$

Contour plots of the flowfield Pitot pressure, p_T, and total temperature, T_0, distributions sampled during the characterisation runs are presented in Figures 7 and 8, respectively, and are separated into separate subplots according to their Knudsen numbers. In each of these, the solid black circles denote sample coordinates and the larger dot-dashed rings show the outline of the nozzle exit. Note that the vertical offset of the nozzle exit outline visible between p_T and T_0 surveys is due to the separation of the probes on the Pitot rake (see Figure 3).

The contours in each plot were generated using cubic spline interpolation of the original survey data. Referring first to Figure 7a, the previously identified region of uniform core flow is immediately evident, with a large zone of constant p_T manifesting at the centre of the flowfield. The high Knudsen number flowfield (plotted in Figure 7b) was interpolated using a smaller set of characterisation points than the low Kn runs, and as such demonstrates a non-physical rhomboidal flowfield when this interpolation is queried for plotting. Despite this artefact, however, it is still evident that the distribution of p_T in the high Kn runs is far less uniform than those at the low Kn condition. A small region of stable p_T, i.e. featuring variation of less than 15%, is once again visible in the range $0 \leqslant r < 5\,mm$ with a lower peak value of p_T at $r = 0$ than was observed in the low Kn runs.

Contour plots of the flowfield total temperature, T_0, are presented in Figures 8a and 8b for the low and high Kn runs, respectively. Much like the p_T contours discussed previously, the low Kn flowfield demonstrates a uniform region of T_0 in the range $0 \leqslant r \leqslant 20\,mm$, while the high Kn runs demonstrate a far smaller such region which lies in the range $0 \leqslant r < 5\,mm$.

5. CONCLUSIONS

In this paper, a characterisation survey of the Oxford Low Density Tunnel (LDT) has been presented. The operation of the facility has been explained, and installed instrumentation described. A series of flowfield surveys at freestream Knudsen numbers of $0.006\dot{6}$ and 0.02 were performed using an automated traversing mechanism, and the resulting data presented herein.

Flowfield surveys comprised Pitot pressure, p_T, and total temperature, T_0, measurements conducted over several separate runs of the facility. From these data, the conditions in the slip regime, i.e. the flow regime where freestream Knudsen numbers typically lie in the range $0.001 \leqslant Kn \leqslant 0.1$ that the LDT may reliably simulate have been determined.

At the $Kn = 0.006\dot{6}$ condition, a core flow region measuring $\sim\ 20\,mm$ in radius has been identified wherein there is little variation in freestream conditions with respect to radial distance, r, from the nozzle centreline. The $Kn = 0.02$ condition, however, did not feature a core flow region nearly as large, instead manifesting peaks in p_T and T_0 which decreased sharply with increasing r (it was observed that p_T readings decreased to half their centreline value at $r \approx 15\,mm$). A small region of low variation ($< 15\%$) was noticeable near $r = 0\,mm$, but extended less than $5\,mm$ from the nozzle centreline.

Estimates of the core flow Mach number $15\,mm$ downstream of the nozzle exit were calculated from experimental measurements for each of the two flow conditions. These val-

ues were shown to lie in the range of Ma which may be considered hypersonic, and were then used to both determine and control the freestream Knudsen number in subsequent LDT runs. Axial surveys of the LDT plume have also previously been undertaken, but are outwith the scope of this paper.

The size of the uniform core flow region in the low Kn runs was found to be sufficient for probes and test articles measuring up to $\sim 40\,mm$ in diameter, while that of the high Kn runs was found only to be large enough for probes less than $10\,mm$ in diameter. It is important to note here that, since Knudsen number is dependant on both mean free path and representative physical scale, reducing the diameter of a test article would naturally increase the freestream Knudsen number (and vice versa).

Additionally, the degree of scatter in experimental results was noticeably higher in the $Kn = 0.02$ runs than those performed at $Kn = 0.0066$ (although it must be noted that fewer runs were performed at the higher Knudsen number condition, which likely contributed to the scatter).

Although the size of the core flow in the high Kn runs was comparatively small compared to that of the low Kn runs, this condition is still useful in the study of re-entry aerothermodynamics. Unlike the low Kn runs, any future experiments performed at the high Kn condition will require more extensive post-processing in order to compensate for the variation of freestream conditions in the core flow region. Such post-processing will likely require DSMC or slip-boundary CFD simulations to be performed with the observed variation in core flow variables being input as a boundary profile. As such, the high Kn may be utilised for the same types of experiments as its low Kn counterpart, albeit with added computational expense.

Overall, it may be concluded that the refurbishment of the LDT has been successful, and that the facility is suitable for the study of hypersonic aerothermodynamics in the slip regime.

6. REFERENCES

[1] Parul Agrawal, Steven A Sepka, Jose F. Aliaga, Ethiraj Venkatapathy, and Jamshid A. Samareh, "Thermal Soak Analysis of Earth Entry Vehicles," *43rd AIAA Thermophysics Conference*, , no. June, pp. 1–16, 2012.

[2] John David Anderson, *Hypersonic and high-temperature gas dynamics*, Reston, Va. : American Institute of Aeronautics and Astronautics, Reston, Va., 2nd ed.. edition, 2006.

[3] Agung Widodo and David Buttsworth, "Stagnation temperature in a cold hypersonic flow produced by a light free piston compression facility," *Experiments in Fluids*, vol. 54, no. 4, 2013.

[4] Greg Dahlen, "Cone Drag in the Transition from Contiuum to Free Molecular Flow," Tech. Rep., England, UK, 1984.

[5] Andrew Owen, *Experimental Studies of the Hypersonic, Low Density, Aerodynamics of Re-entry Vehicles*, Ph.D. thesis, Oxford, UK, 1997.